J. Chem. Sci. Vol. 126, No. 2, March 2014, pp. 361–372.

Novel nanostructured CeO_2 as efficient catalyst for energy and environmental applications

SUMANTA KUMAR MEHER[a,b] and G RANGA RAO[a,*]

[a]Department of Chemistry, Indian Institute of Technology Madras, Chennai 600 036, India
[b]Department of Chemistry, Malaviya National Institute of Technology Jaipur, Rajasthan 302 017, India
e-mail: grrao@iitm.ac.in

MS received 4 July 2013; revised 22 October 2013; accepted 26 October 2013

Abstract. We report here versatile methods to engineer the microstructure and understand the fundamental physicochemical properties of CeO_2 to improve its catalytic viability for practical applications. In this context, different morphologies of CeO_2 are synthesized using tailored homogeneous precipitation methods and characterized by XRD, BET, SEM and TPR methods. The shuttle-shaped CeO_2 prepared under hydrothermal condition shows higher surface area and low-temperature reducibility. The 0.5 wt% Pt-impregnated shuttle-shaped CeO_2 shows lower-temperature CO oxidation behaviour as compared to its bulk-like CeO_2 (with 0.5 wt% Pt) counterpart, synthesized by conventional-reflux method. Further, nanorod morphology of CeO_2 prepared with Cl^-as counter ion shows lower-temperature oxidation of soot as compared to the mesoflower morphology of CeO_2, prepared with NO_3^- as counter ion in the reaction medium. Further, linear sweep voltammetry, chronopotentiometry and CO-stripping voltammetry studies are performed to evaluate the promoting activity of CeO_2 to Pt/C for ethanol electro-oxidation reaction in acidic media. Results show that CeO_2 provides active triple-phase-interfacial sites for suitable adsorption of OH species which effectively oxidize the CO_{ads} on Pt/C. The results presented here are significant in the context of understanding the physicochemical fine prints of CeO_2 and CeO_2 based hetero-nanocomposites for their suitability to important catalytic and energy-related applications.

Keywords. CeO_2; morphology; catalysis; soot oxidation; CO oxidation; ethanol electro-oxidation.

1. Introduction

In the developing world of rapid industrialization and growing population, it is essential to address the issues in pollution control and renewable energy due to rapidly depleting fossil fuels and heavy toxification of the environment by combustion-based technologies. Automobile and industrial exhausts such as carcinogenic soot particles and poisonous CO molecules are major environmental concerns and the major challenge is the efficient abatement of soot and CO by catalytic oxidation.[1,2] Regarding the issue of CO, homogenous oxidation of CO requires very high temperature (~700°C), which is practically not feasible. The issue is down to the spin forbidden situation, i.e., the reactants have total spin S = 1 (triplet ground state of O_2) and the product (CO_2) has spin S = 0. However, for a dissociated O_2, the individually adsorbed O atoms are in spin S = 0 states, and thus the reaction becomes energetically feasible.[2,3] Dissociation of O_2 can only happen on a heterogeneous surface; hence oxidation of CO by a catalytic route is essential. In this context, numerous metal–metal oxide combinations have been looked into which show substantial activity for oxidation of CO by O_2.[2–6] Among the vast possibilities of catalysts, Pt/CeO_2 has been the most studied due to the significant chemical proportionation between Pt and CeO_2 which results in the excellent stability, reactivity and activity of the catalyst for CO oxidation.[7–9] Further, strong Pt–CeO_2 interaction avoids sintering of Pt crystallites during reactions at extreme thermal conditions. Excellent redox behaviour (Ce^{4+}/Ce^{3+} redox transition), large number/concentration of oxygen vacancies, significant oxygen mobility and high oxygen storage capacity also make CeO_2 an ideal support of Pt for CO oxidation under cyclic conditions.[10–12] Structural modification of metals and metal oxides in nano- as well as microscale dimension influencing the surface atom densities, electronic structure and chemical reactivity is well-known.[13–16] In this context, microstructurally designed CeO_2 with specifically oriented crystals, small crystallite size and large number of accessible surface active sites can be more active as a catalyst than bulk CeO_2. For instance, nanowires and nanorods of CeO_2 predominantly exposing (100) and (110) faces are more

*For correspondence

active for CO oxidation than nanoparticles of CeO_2 with (111) exposed surface.[17] Further, suitable microstructure of CeO_2 can limit sintering of Pt crystallites during extreme reaction conditions.

Regarding the issue of soot, complete oxidation of soot occurs only above 800°C, which is impossible to be achieved under practical reaction conditions. Further, kinetics of soot oxidation over a catalyst is very slow. Large size particles of soot also make it difficult to be mobilized on active catalyst surfaces.[1] Studies show that heterogeneous oxidation of soot proceeds through transfer of molecular oxygen from the catalyst to soot. Hence, materials which can 'oscillate' between two oxidation states are ideal for oxidation of soot. In this context, CeO_2 which easily undergoes Ce^{4+}/Ce^{3+} redox transition shows exceptional activity towards oxidation of soot. Rigorous studies by Makkee and co-workers suggest that active oxygen transfer to soot is crucial for soot oxidation activity of CeO_2.[18,19] Further, the vacancies on CeO_2 promote the spilling of active oxygen to neighbouring soot particles.[1,18,19] Hence, increasing the amount of reactive oxygen on CeO_2 surface promotes facile oxidation of soot. In this context, the most significant approach has been towards generation of oxygen vacancy by doping with alkali, transition and noble metals. However, a recent report by Guzman *et al*., shows that only nanocrystalline CeO_2 stabilizes O_2 as active superoxide and peroxide species, whereas the bulk CeO_2 stabilizes molecular O_2.[20] Furthermore, only nanocrystalline CeO_2 supplies reactive oxygen in the form of surface η^1 superoxide species and peroxide adspecies.[20] This as a whole indicates that any processing condition which favours formation of more desired oxygen vacancies can result in enhanced activity of CeO_2 for soot oxidation. In the above connection, suitable nano-structurization and appropriate microstructural engineering of CeO_2 with larger accessible surfaces, high thermal stability and more oxygen vacancy is the best approach to achieve facile catalytic oxidation of soot.

On the energy front, direct alcohol fuel cells (DAFCs) have emerged as one of the most versatile devices for practical application in transport and portable device applications because of their higher energy density, use of liquid fuel (methanol and ethanol), low operating cost and compact design.[21–23] Studies confirm that Pt is the most active electrocatalyst for electrooxidation of alcohol in DAFCs.[24] However, during electrooxidation process of alcohol, carbonaceous species such as CO are produced as reaction intermediates which heavily poison the Pt surface and worsen the performance of Pt-based catalysts during long-term operation of the device.[25]

Metal oxides are highly oxophilic and are known to allow activation of water at lower potentials. Hence, they are prone to adsorption of oxygenated species such as OH at lower potential which can promote the electrooxidation of CO_{ads} to CO_2 via the well-known bifunctional mechanism.[26] In this context, various metal oxides such as WO_3, RuO_2, MgO, ZrO_2, MoO_3, MoO_2, Nb_2O_5, V_2O_5, TiO_2, and CeO_2 in combination with carbon are reported as highly promising electrocatalysts which show significant tolerance to CO poisoning.[27–35] CeO_2 is one of the most important electrocatalysts due to its high surface area, sizable surface defects and higher oxygen storage capacity. Due to suitable surface properties, CeO_2 has a tendency to stabilize the dispersed Pt, which favours sufficient OH_{ads} species available at lower potential to oxidize majority of CO_{ads} species during electrooxidation of alcohol.[30] In this context, several reports in the literature show excellent promotional activities of CeO_2 for methanol electrooxidation reaction.[30,36,37] Although, the promoting activity of CeO_2 for electrooxidation of ethanol in alkaline media has been well-reported,[38] its promotional efficiency in acidic media is rarely studied, which needs serious attention.

Hence, understanding the energetic and molecular designing of suitable CeO_2-based catalysts with economic and environmental viability is central to dealing with the energy and environmental issues as outlined above. These issues are addressed in the present study of tailored surface microstructures of CeO_2 with uniquely combined surface and bulk properties.

2. Experimental

2.1 *Chemicals*

Analytical grade $Ce(NO_3)_3{\cdot}6H_2O$ (99.9%, SD Fine, India), $CeCl_3{\cdot}7H_2O$ (99.9%, Sigma), cetyltrimethylammonium bromide (CTAB) (Sigma), poly(ethylene glycol)-poly(propylene glycol)-poly(ethylene glycol) (P123, Sigma-Aldrich) with a molecular weight of 5800 g, urea (99.9%, Thomas-Baker), chloroplatinic acid hexahydrate ($H_2PtCl_6{\cdot}6H_2O$, Sigma-Aldrich) with $\geq$ 37.50% Pt basis and Nafion (5 wt% solution in a mixture of lower aliphatic alcohols, Sigma-Aldrich) were used as received. Laboratory prepared triple distilled water was used during all the experimental processes.

2.2 *Preparation of CeO_2 samples with different microstructures*

In a typical synthesis, 40 mmol of $Ce(NO_3)_3{\cdot}6H_2O$ was dissolved in 200 mL of water, and the resulting

solution was added dropwise to 100 mL of 2 mmol P123 solution. After stirring the solution for 1 h, 160 mmol of solid urea was added, and further stirred for 3 h. The resulting solution was then divided into two equal halves, one half was transferred to a stainless steel autoclave with an inside Teflon liner of 250 mL capacity and subjected to heating at 120°C for 24 h. The other half was transferred to a round bottom flask of 250 ml capacity and subjected to heating under reflux condition at 120°C for 24 h. After reactions under both hydrothermal and reflux conditions, the reaction mixtures were allowed to cool to room temperature and resulting white solid precipitates were concentrated by centrifugation at 3000 rpm. The products were then repeatedly washed with triple distilled water followed by mixture of absolute ethanol and water and finally with absolute ethanol several times. The precursor samples were then dried in a vacuum oven at 60°C for 24 h. The dried samples were finally calcined at 400°C for 3 h in flowing air. The samples prepared under hydrothermal and reflux conditions are denoted as CeO_2-H and CeO_2-R, respectively.

Another set of CeO_2 samples were prepared by using different precursors of Ce in the reaction under homogeneous precipitation condition. In a typical synthesis, 20 mmol of a cerium salt (cerium nitrate or cerium chloride) was dissolved in 100 ml of triple distilled water and was added dropwise to 100 mL of 10 mmol aqueous CTAB solution. The solution was stirred for 1 h and to that 80 mmol of solid urea was added and stirred for additional 3 h. The solution was then transferred to a round bottom flask of 250 ml capacity, and subjected to refluxing at 120°C for 24 h with constant stirring. The product was then allowed to cool to room temperature and after ageing for 24 h, the resulting white colour precipitate (precursor) was separated by centrifugation at 3000 rpm. The precursor was then repeatedly washed with triple distilled water followed by mixture of absolute ethanol and water and finally with absolute ethanol for several times. The precipitate was then dried in a vacuum oven at 60°C overnight, and the dried sample was calcined at 400°C for 3 h in flowing air. The samples prepared using nitrate and chloride precursors are denoted as CeO_2-N and CeO_2-C, respectively.

2.3 *Preparation of 0.5 wt% Pt-loaded CeO_2 by impregnation method*

To prepare 0.5 wt% Pt-loaded CeO_2 samples, 500 mg of CeO_2-H (or CeO_2-R) sample was constantly stirred for 12 h in water for thorough dispersion. Suitable amount of aqueous $H_2PtCl_6{\cdot}6H_2O$ was then added dropwise and the resultant mixture was slowly heated until dryness. The solid product was dried under vacuum at 60°C overnight and then calcined at 500°C (heating ramp = 5°C min^{-1}) for 3 h in flowing air. The 0.5 wt% Pt-loaded CeO_2-H and CeO_2-R samples were designated as Pt-CeO_2-H and Pt-CeO_2-R, respectively.

2.4 *Preparation of CeO_2-based electrocatalyst composites*

For the preparation of a 20 wt% CeO_2-based Pt/CeO_2-C electrocatalyst, 20 mg of CeO_2 and 100 mg of Vulcan XC-72 carbon black were ultrasonically dispersed in 100 mL of ethylene glycol (EG)-isopropyl alcohol (IPA) mixture solution (V/V = 4:1). Appropriate amount of 0.1 M $H_2PtCl_6{\cdot}6H_2O$-EG solution was then added to the above mixture, which was further sonicated for 15 min and stirred for 6 h. The pH of the mixture ink was adjusted to ~10 by 1 M KOH-EG solution and was then treated with microwave radiation for 50 s in order to achieve complete reduction of $H_2PtCl_6{\cdot}6H_2O$ to Pt. After cooling to room temperature, pH of the mixture ink was then adjusted to ~4 by 0.1 M HNO_3. After stirring the solution mixture for 12 h, the resultant product was filtered out and then washed with water, followed by acetone for several times. Finally, the resultant product was dried under vacuum at 60°C overnight. The Pt/C electrocatalyst was prepared by similar procedure, but without CeO_2. The amount of Pt in the electrocatalyst samples was fixed at 20 wt%.

2.5 *Preparation of working electrode and electrochemical measurements*

The working electrodes were fabricated from the ink prepared by ultrasonically dispersing the electrocatalysts (Pt/C and Pt/CeO_2/C) in 1.0 mL of distilled water and 0.1 mL of Nafion solution for 30 min. An appropriate volume of the ink composite was then spread onto a mirror-finished glassy carbon electrode of 6 mm diameter using a micropipette tip. A well-dispersed layer of composite material on the glassy carbon electrode was obtained by drying the ink at 40°C in vacuum. The amount of Pt loading was fixed at 28 μg cm^{-2}. Electrochemical measurements were performed with a conventional three-electrode configuration in a CHI 7081C electrochemical workstation. A platinum foil (area = 1 cm^2) and an Ag/AgCl electrode were used as the counter and reference electrodes, respectively. A solution of 0.5 M H_2SO_4 and 1 M C_2H_5OH was purged with high-pure Ar for 30 min under constant stirring, and was taken as the test solution for electrochemical study. For CO stripping voltammetry study, a 0.5 M H_2SO_4 solution was purged with ultrapure Ar for 30 min and

then with CO (0.1% CO in Ar) for 120 min under a fixed potential of 0.0 V vs Ag/AgCl. After purging the solution with Ar for 30 min under a potential of 0.0 V vs Ag/AgCl, the CO stripping voltammetry patterns were recorded at a potential scan rate of 20 mV s^{-1}.

2.6 *Soot oxidation measurements*

Soot oxidation activity measurements were carried out by thermogravimetry analysis (TGA) method in a 'tight contact' mode with CeO_2:soot at 4:1 wt/wt. An appropriate amount of CeO_2-soot mixture was finely ground in an agate mortar and subjected to thermal analysis up to 800°C at a heating rate of 10°C min^{-1} under air flow (50 ml min^{-1}). The model soot used in this study was Columbian Carbon (CC).

2.7 *CO oxidation measurements*

For a typical CO oxidation activity measurement, ~40 mg of Pt/CeO_2 sample was placed in a U-shaped quartz micro-reactor (internal diameter of 4 mm) and subjected to pretreatment at 350°C under a flowing gas mixture of 5% O_2/95% Ar, at 40 mL min^{-1} for 30 min. The sample was then cooled to 150°C and then exposd to 47.5% H_2 in Ar for 1 h. After cooling the sample to room temperature, the CO oxidation reaction was performed under a gas flow with gas hourly space velocity (GHSV) of ~75,000 mL g^{-1} h^{-1}. The temperature ramp was maintained at 2°C min^{-1} and the feed gas used for the reaction was 1.0 vol.% CO and 4.0 vol.% O_2 in Ar. An online mass spectrometer (Hyden Analytical HPR20) operating at an acquisition time of the order of 1 point for every 12 s was used to analyse the products. Conversion of CO was calculated from the decrease in the characteristic $m/z = 28$ signal corrected for the CO_2 cracking pattern.

2.8 *Physicochemical characterization*

Thermogravimetry analyses were performed on a TGA Q500 V20.10 Build 36 (TA make) instrument. Powder X-ray diffraction (PXRD) patterns were obtained on a Bruker AXS D8 Advance diffractometer at a scan rate of 0.01° s^{-1}, using Cu Kα ($\lambda = 0.15408$ nm) radiation generated at 40 kV, 30 mA. Crystallite sizes of the samples were calculated using Scherrer equation, $D = K\lambda/(\beta \cos \theta)$, where D is the linear dimension of the particle (particle size), K is the spherical shape factor (0.89), and β is the full width at half-maximum height (FWHM) of the peak. The multipoint nitrogen adsorption-desorption experiments were carried out at 77 K in a Micromeritics ASAP 2020 instrument based on Brunauer-Emmett-Teller (BET) gas adsorption method. Respective samples were degassed at 100°C for 2 h, followed by 150°C for 10 h in a dynamic vacuum before physisorption measurements. Porosity distributions in the samples were generated from desorption branches of the adsorption–desorption isotherms using Barrett-Joyner-Halenda (BJH) method and a cylindrical pore model.

Temperature programmed reduction (TPR) measurements were carried out in a Micromeritics Chemisorb 2750 TPD/TPR system. For a typical H_2-TPR experiment, 80 mg of the sample was loaded in a U-shaped quartz tube, and pretreated at 250°C in flowing 20% O_2/He (25 mL/min) gas mixture for 1 h. The sample was cooled to room temperature under flowing He, and then heated up to 850°C at a temperature ramp of 10°C min^{-1}, under the flow of 5% H_2/He mixture (20 mL/min). The TPR patterns were recorded using a thermal conductivity detector.

High Resolution Scanning Electron Microscopy (HRSEM) measurements were carried out using a field emission gun-equipped FEI Quanta 200 microscope. The sample powders were dispersed in ethanol and then spread onto carbon tape before mounting on the sample holder for analysis.

3. Results and discussion

3.1 *Morphology dependent CO oxidation activity of CeO_2*

The PXRD patterns of CeO_2-H and CeO_2-R samples prepared under hydrothermal and reflux conditions, respectively, are shown in figure 1, which shows prominent peaks at 28.6°, 33.1°, 47.5°, 56.3° and 59.1°, corresponding to the (111), (200), (220), (311) and (222) planes of FCC type CeO_2. Formation of CeO_2 under homogeneous precipitation condition followed by thermal treatment undergoes the following reaction steps:[30]

$$NH_2CONH_2 \xrightarrow[hydrolysis]{120^\circ C} NH_4^+ + NCO^-$$
$$NCO^- + 3H_2O \rightarrow HCO_3^- + NH_4^+ + OH^-$$
$$HCO_3^- \rightarrow CO_3^{2-} + H^+$$
$$Ce^{3+} + OH^- + CO_3^{2-} \rightarrow Ce(CO_3)_2O \cdot H_2O$$
$$Ce\,(CO_3)_2\,O \cdot H_2O \xrightarrow{400^\circ C/Air} CeO_2.$$

The PXRD patterns are devoid of any major secondary peaks which illustrate the high purity of CeO_2 samples. However, there is a clear difference in the broadness and intensity of CeO_2-H and CeO_2-R samples,

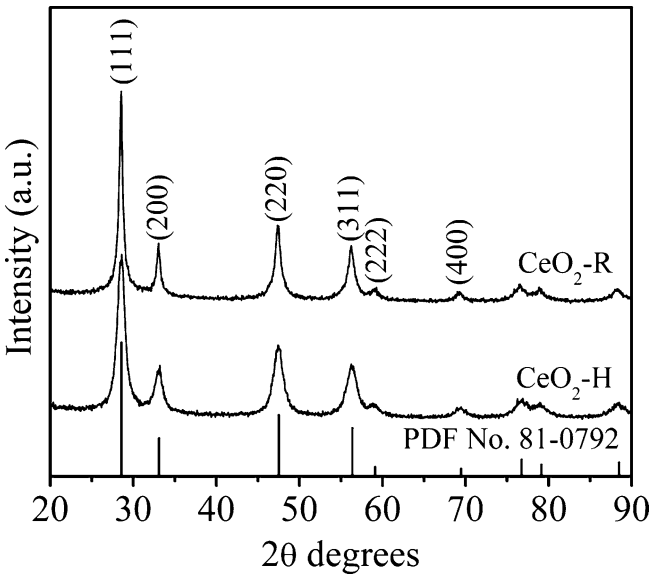

Figure 1. PXRD patterns of CeO_2-R and CeO_2-H samples.

which is attributed to the difference in the size of the crystallites in the samples. The PXRD peaks of CeO_2-R sample are sharper as well as more intense compared to those of CeO_2-H sample, which obviously indicates that the CeO_2-R sample is more crystalline than the CeO_2-H sample. The calculated (using Scherrer equation) average crystallite sizes of CeO_2-R and CeO_2-H samples are found to be ~16.9 nm and 6.8 nm, respectively. It seems that homogeneous precipitation under hydrothermal condition provides more ideal chemical environment for uniform crystal growth compared to the reflux condition.

Surface morphological characteristics of the CeO_2-R and CeO_2-H samples are seen in their FESEM images in figure 2a and 2b, respectively. The CeO_2-R sample shows randomly arranged structures made up of microplates (shown with red colour arrow), whereas the CeO_2-H sample shows rather uniform shuttle-like morphology made up of nanosize rods (shown with blue colour arrow). It gives an impression that unlike reflux condition under conventional heat treatment approach, hydrothermal condition offers a more suitable environment for uniform nanorod growth and nanorod self-assembly to distinctive surface microstructure of CeO_2.

Physicochemical characteristics of the two CeO_2 samples were investigated by BET analysis, and the results (N_2 adsorption-desorption isotherms and pore size distribution plots) are presented in figure 3. The isotherms are type-IV in nature with H3 type hysteresis loops.[39] This essentially indicates the presence of micro- and mesopores in the CeO_2 samples and the pores are likely to be slit-shaped which may be due to the agglomerated microstructures forming the mesostructures. The BJH pore size distribution plots in the inset of figure 3 show that the pores in the CeO_2 samples are bimodal (~2 nm and 6.1–8.3 nm) in nature. However, in the CeO_2-H sample, size distribution of micropores is higher in intensity which clearly indicates added micropores in the CeO_2-H sample as compared to the CeO_2-R sample. Higher N_2 adsorption in the p/p_0 region of 0 to ~0.04 for CeO_2-H sample as compared to the CeO_2-R sample further corroborates the presence of more number of micropores in the CeO_2-H sample. The good arrangement of nanorods can be the possible reason for higher microporosity in the CeO_2-H sample. The BET surface area and BJH pore volume of CeO_2-H sample are found to be ~109 $m^2\ g^{-1}$ and 0.11 $cm^3\ g^{-1}$, respectively; whereas for CeO_2-R sample, the values are found to be 95 $m^2\ g^{-1}$ and 0.089 $cm^3\ g^{-1}$, respectively.

CeO_2 is known as an excellent redox catalyst due to easy interconversion of Ce^{4+} to Ce^{3+} and vice versa. In this context, lower temperature reducibility is the most important property which explains the improved catalytic efficiency of CeO_2.[40] The H_2-reduction (H_2-TPR)

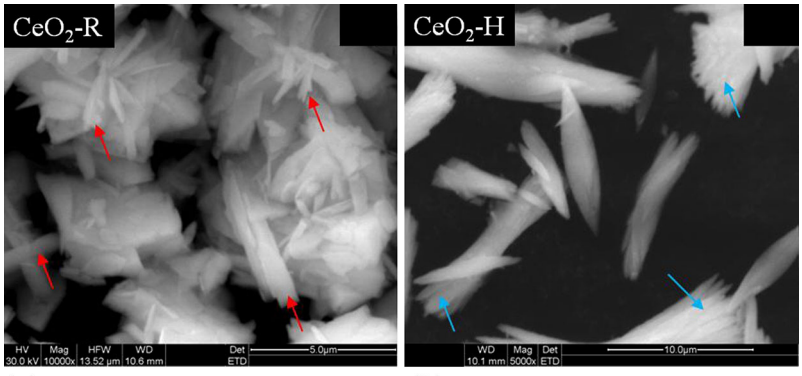

(a) **(b)**

Figure 2. FESEM images of (**a**) CeO_2-R and (**b**) CeO_2-H samples.

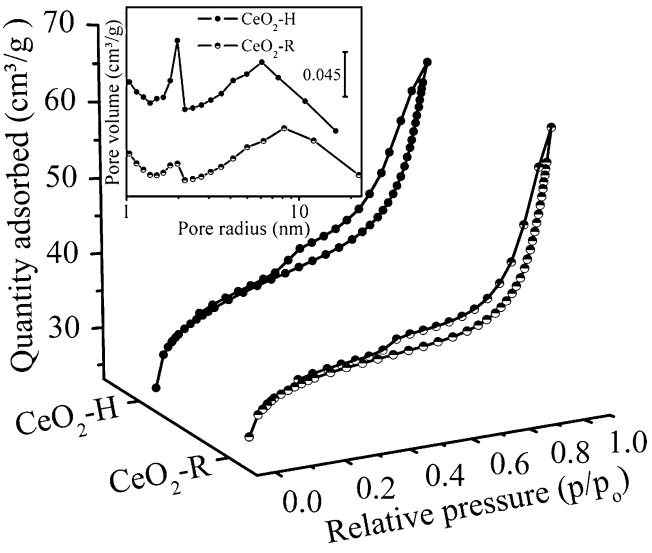

Figure 3. BET isotherms of the CeO_2-H and CeO_2-R samples; inset shows the corresponding pore size distribution profiles of the samples.

profiles of CeO_2-H and CeO_2-R samples are presented in figure 4, which shows major reduction peaks at two temperature ranges, i.e., below 600°C and above 600°C, which are due to surface and bulk reduction of CeO_2, respectively.[9,12,30,40] From figure 4, it is seen that the bulk reduction of CeO_2-H and CeO_2-R samples occurs at an almost similar temperature range with a reduction maxima at ~780°C. However, there is a clear difference in the surface reduction behaviour of CeO_2-H and CeO_2-R samples. The CeO_2-H sample shows a highly intense low-temperature reduction peak at ~268°C, whereas the CeO_2-R sample shows a typical surface reduction at ~420°C. This is attributed to the presence of larger size and number of oxygen vacancy clusters on the surface of CeO_2-H sample. This also signifies the presence of higher amount of reactive oxygen species on the surface of CeO_2-H sample as compared to the CeO_2-R sample.[9] Oxygen vacancy clusters essentially facilitate the catalytic activity of CeO_2.[8,9] The different rate of crystal growth under the hydrothermal and reflux reaction conditions is the rationale behind the presence of dissimilar oxygen vacancy clusters in the CeO_2-H and CeO_2-R samples. The marked negative peaks at ~513°C in the reduction profiles of both samples are assigned to liberation of CO and CH_4 during the H_2-reduction of surface carbonates on the CeO_2 samples.[12]

The CeO_2-R and CeO_2-H samples were tested for their catalytic efficiency after impregnating 0.5 wt% of Pt in the samples and the CO oxidation efficiencies of Pt-CeO_2-R and Pt-CeO_2-H samples are presented in figure 5. Microstructural effects of the CeO_2 support as well as the supported Pt crystallites on the CO oxidation efficiencies of Pt-CeO_2 materials is well-known. The mechanism of CO oxidation on Pt-CeO_2 can be written as:[2,3,41]

$$CO + Pt \rightarrow Pt - CO_{(ads)}$$
$$O_{2(g)} + \otimes \rightarrow O_{2(ads)} - \otimes$$
$$O_{2(ads)} - \otimes + \otimes \rightarrow 2O_{(ads)} - \otimes$$
$$Pt - CO_{ads} + O_{(ads)} - \otimes \rightarrow CO_2 + Pt + \otimes,$$

where $\otimes$ symbolizes an individual active site over CeO_2 surface. From figure 5, it is seen that the Pt-CeO_2-R and Pt-CeO_2-H samples oxidize 100% of CO in the

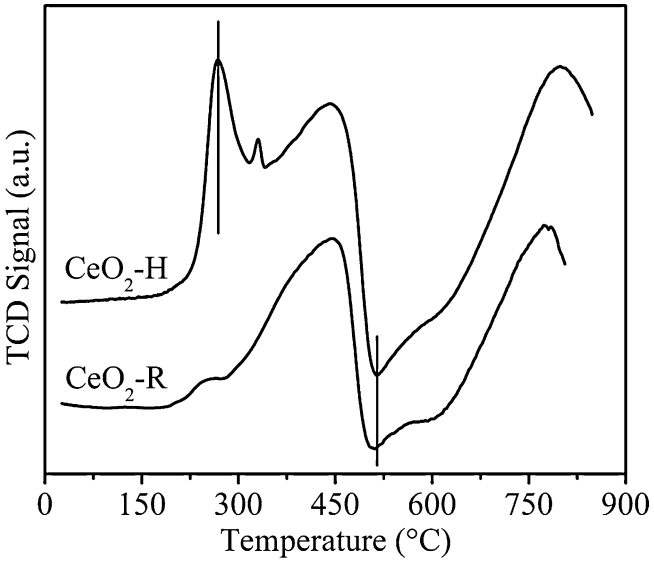

Figure 4. H_2-TPR profiles of CeO_2-R and CeO_2-H samples.

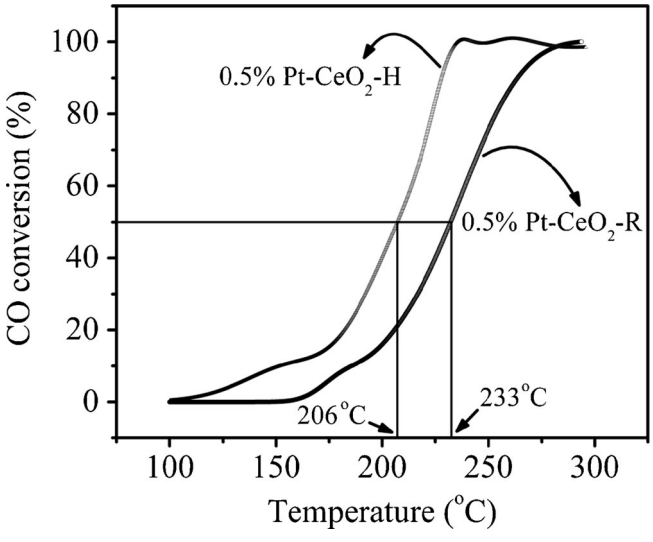

Figure 5. Conversion of CO in the presence of O_2 over 0.5 wt% Pt loaded (impregnation method) on CeO_2-R and CeO_2-H samples.

temperature range of ~150–300°C. However, 100% oxidation of CO on Pt-CeO_2-R and Pt-CeO_2-H samples occurs at ~286°C and ~237°C with light-off temperatures (temperature at 50% conversion of CO, $T_{1/2}$) at 206°C and 233°C, respectively. It is known that the Pt/CeO_2 interfacial sites are more responsible for the oxidation of CO.[9] In this context, it is obvious that the characteristic Pt/CeO_2 interfacial sites in the Pt-CeO_2-R and Pt-CeO_2-H samples are different due to different surface morphologies of CeO_2-R and CeO_2-H. In fact, due to the presence of higher amount/density and larger size of oxygen vacancy clusters in CeO_2-H sample, interfacial sites in Pt/CeO_2-H sample are more in number and highly active compared to those in Pt/CeO_2-R sample. The oxygen vacancy clusters on CeO_2 are in fact responsible for facile adsorption and easy diffusion of oxygen from the bulk to the surface of CeO_2 and lead to lower temperature oxidation of CO.[8,9,42] The high surface area of CeO_2-H sample provides added active sites for interaction with Pt and reaction with CO. Since the Pt loading has been performed under similar procedure and experimental conditions, the effect of different oxidation states of Pt on the CO oxidation can be neglected. These results truly substantiate the significant microstructural effect of CeO_2 on the CO oxidation efficiency of Pt–CeO_2 heteronanocomposites.

3.2 *Morphology dependent soot oxidation activity of CeO_2*

Surface morphologies of CeO_2-N and CeO_2-C samples prepared using nitrate and chloride precursors (or counter ions), respectively, are presented in the FESEM images in figure 6. The CeO_2-N sample shows mesoflower type surface morphology which is made up of orientally attached microplate structures. In contrast, the CeO_2-C sample shows freely-dispersed nanorod morphology. Barring the nature of counter anions (Cl^- and NO_3^-), the other parameters of the reactions to prepare CeO_2-N and CeO_2-C samples are essentially the same. In this context, the different surface morphologies of CeO_2-N and CeO_2-C samples are supposed to occur due to significant effect of Cl^- and NO_3^- on the nucleation and crystal growth of the product.[12] Preferential adsorption of anions on specific crystallographic planes which control the dynamics of crystal growth process to form specific surface morphology of the materials is well-known. In this context, selective adsorption of Cl^- and NO_3^- anions assists the kinetic growth of precursors to form the small nanorods and microplates, which after suitable self-assembly process form the final morphologies of CeO_2-C and CeO_2-N, respectively.

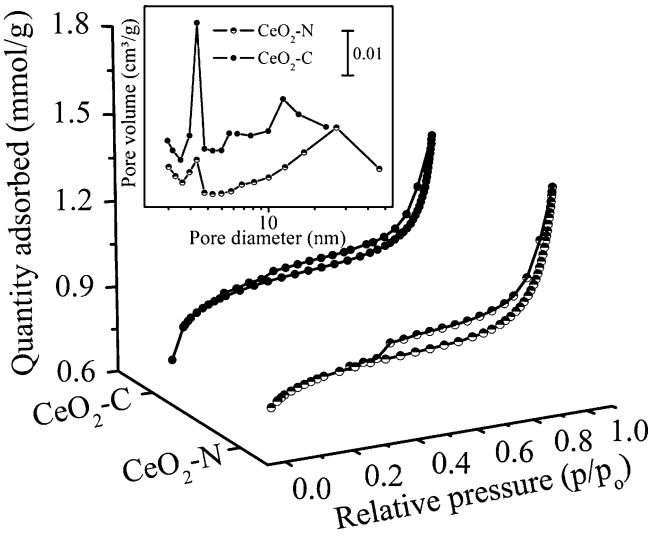

Figure 7. BET isotherms of the CeO_2-C and CeO_2-N samples; inset shows the corresponding pore size distribution profiles of the samples.

Characteristic N_2 adsorption–desorption isotherms and pore size distribution profiles of CeO_2-C and CeO_2-N samples are presented in figure 7. Both the samples show type-IV isotherms with H3 type hysteresis loops, characteristics of slit-shaped pores

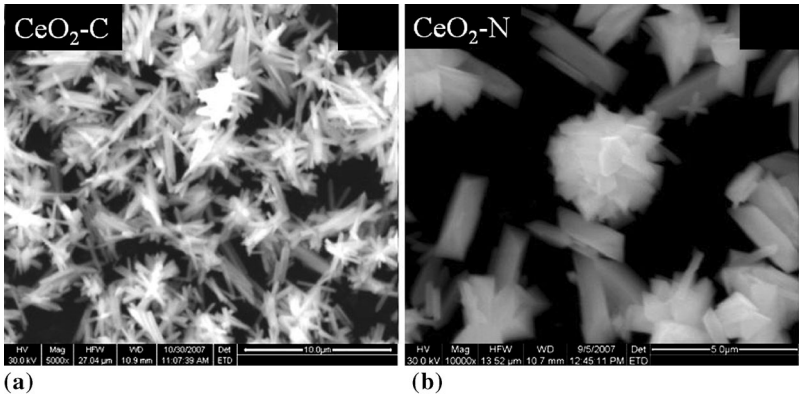

(a) **(b)**

Figure 6. FESEM images of (**a**) CeO_2-C and (**b**) CeO_2-N samples.

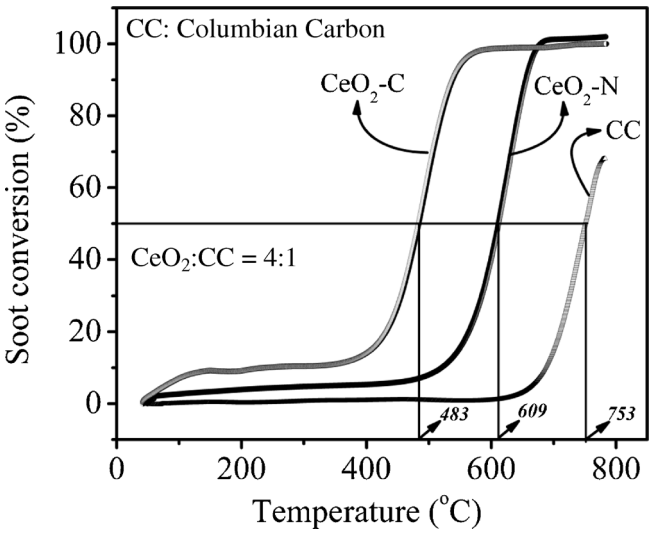

Figure 8. Oxidation of Columbian Carbon (CC, soot) on CeO_2-C and CeO_2-N samples.

due to aggregates of plate-like particles in the CeO_2 samples.[12,39] The BJH pore size distribution profiles showed in the inset of figure 7 demonstrate the presence of multimodal pores in the CeO_2-C and CeO_2-N samples. The estimated BET surface area of the CeO_2-C and CeO_2-N samples are found to be ~106 and ~71 m^2/g, respectively, with corresponding BJH pore volume of ~0.07 and ~0.05 cm^3/g. The surface area of CeO_2-C being significantly higher, it is supposed to provide more number of surface active sites for catalytic reaction. In this context, both the CeO_2 samples were investigated for their catalytic efficiency to soot (Columbian Carbon, CC) oxidation reaction and the results are presented in figure 8.

Soot oxidation profiles in figure 8 show that both the CeO_2-C and CeO_2-N samples oxidize soot at lower temperature than the temperature at which oxidation of soot occurs by O_2. It is significant to note that only ~70% of soot gets oxidized by O_2 at a very high temperature of ~800°C. However, the CeO_2 samples catalytically oxidize 100% of soot at significantly lower temperature. Further, soot oxidation efficiencies of CeO_2-C and CeO_2-N samples are very different. For instance, 100% soot oxidation on CeO_2-C sample occurs at ~581°C with a $T_{1/2}$ (temperature at 50% conversion of soot) at ~483°C. In contrast, 100% soot oxidation on CeO_2-N sample occurs at ~690°C with a $T_{1/2}$ at ~609°C. Further, the onset temperature of soot oxidation on CeO_2-C is drastically lower than that on CeO_2-N sample. Literature shows that active oxygen of CeO_2 surface is spilled onto the surface of soot particles and gets adsorbed at the active carbon site during catalytic oxidation of soot.[43,44] A recent study by Machida *et al*. shows that the catalytic soot oxidation reaction can also follow a mechanism where adsorption of superoxides and soot at the three-phase boundary and active lattice oxygen and soot at the CeO_2/soot interface occurs.[45] Hence, the high catalytic soot oxidation efficiency of CeO_2-C and CeO_2-N samples is attributed to the facile generation of highly active oxygen from the lattice due to the Ce^{3+}/Ce^{4+}-induced oxygen exchange between O_2 from air and O_2 in the CeO_2 framework.[12,45] The superior catalytic efficiency of CeO_2-C is attributed to the high surface area and possible presence of more number of large-size oxygen vacancy clusters which promote the formation of active oxygen, superoxide (O^{2-}) in the vicinity of soot, and facile electron transfer from Ce^{3+} to soot. This can be represented as:[12]

$$Ce^{3+} - O_{vac} + O_2 \rightarrow Ce^{4+} - \left(O - O^{-}\right).$$

These results corroborate previous studies on the CeO_2 nanorods which show that the nanorods surround numerous defects on its surface, which promote the activation of adsorbed oxygen to form superoxides.[12] From this study, it is clear that the Cl^- ion induces more oxygen vacancy (defects) in CeO_2 compared to the NO_3^- ion during homogeneous precipitation synthesis of CeO_2. The facile way of tuning the microstructure of CeO_2 by specific counter anions and the morphology-controlled catalytic activity of CeO_2 make this study a future perspective for numerous practical applications.

3.3 *Promoting activity of CeO_2 for ethanol electrooxidation on Pt/C*

To assess the promoting activity of CeO_2 for energy application, the ethanol electrooxidation efficiency of $Pt/CeO_2/C$ was compared with that of Pt/C. In this context, the corresponding PXRD patterns of Pt/C and $Pt/CeO_2/C$ samples are shown in figure 9. Both the samples show diffraction peaks at 2θ values of 39.8°, 46.3°, 67.6° and 81.4°, corresponding to the (111), (200), (220), and (331) planes of fcc type Pt crystallites.[30] The $Pt/CeO_2/C$ sample also shows peaks corresponding to fcc type CeO_2 as indexed in figure 9. The presence of Vulcan XC-72 carbon support is confirmed by the broad peaks at a 2θ value of ~24.9° in both the Pt/C and $Pt/CeO_2/C$ samples. Diffraction peaks of Pt in $Pt/CeO_2/C$ are noticeably broader and lower in intensity. This is ascribed to the smaller crystallite size and high dispersion of Pt in the CeO_2-modified Pt/C sample. Studies show that due to its suitable surface properties, CeO_2 promotes uniform

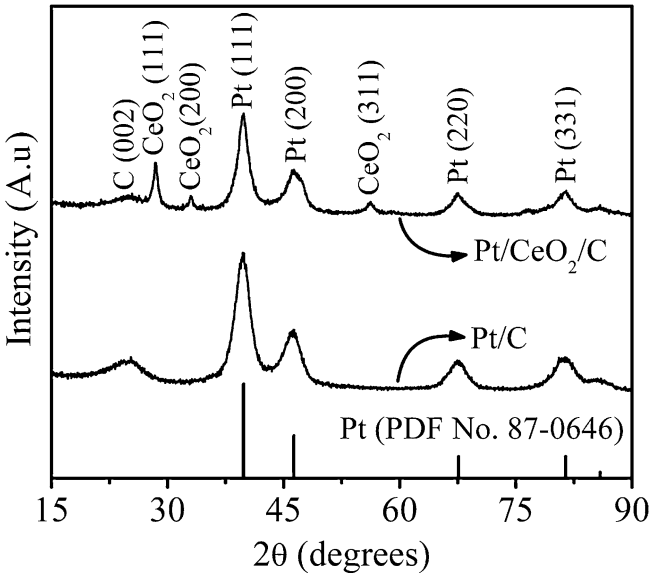

Figure 9. PXRD patterns of Pt/C and $Pt/CeO_2/C$ samples.

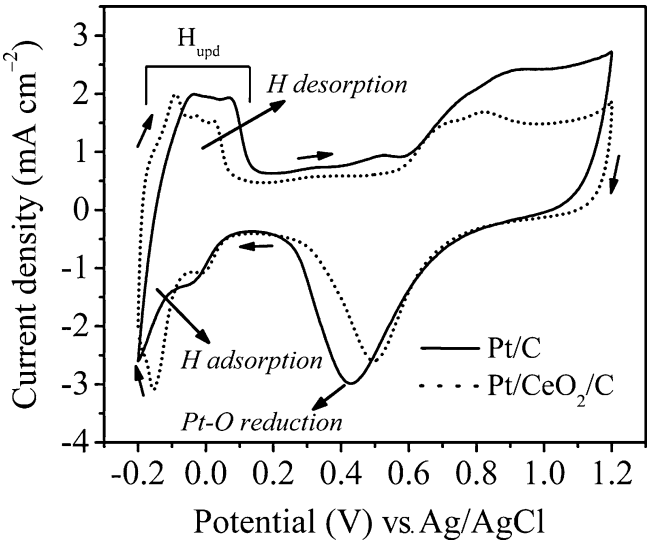

Figure 10. Comparative cyclic voltammograms (scan rate = 20 mV s^{-1}) of Pt/C and $Pt/CeO_2/C$ samples in H_2SO_4 (0.5 mol L^{-1}) solution.

dispersion and miniaturization of Pt crystallites. Similar observation here corroborates the promoting activity of CeO_2 for dispersion and miniaturization of Pt crystallites in $Pt/CeO_2/C$ electrocatalyst sample. The above assumption is further supported by the calculated (Scherrer equation) crystallite sizes of Pt (from (220) diffraction) in Pt/C and $Pt/CeO_2/C$ samples, which are found to be ~4.3 nm and ~3.5 nm, respectively. Here, ethylene glycol acts as a reducing agent for conversion of $H_2PtCl_6{\cdot}6H_2O$ to Pt and also enhance the dispersion of CeO_2 on Vulcan XC-72 support. Uniform dispersion and miniaturization of Pt crystallites are also facilitated by gradient-free heating during microwave treatment.[46]

Electrocatalytic efficiencies of the Pt/C and CeO_2-promoted Pt/C electrocatalysts were evaluated by linear sweep voltammetry, chronopotentiometry and CO stripping voltammetry measurements in an acidic medium (0.5 mol L^{-1} H_2SO_4 solution). To evaluate the characteristics of dispersed Pt, the Pt/C and $Pt/CeO_2/C$ sample electrodes were subjected to cyclic voltammetry (CV) measurements and the resultant profiles are shown in figure 10. The typical CV profiles show peaks corresponding to hydrogen adsorption/desorption (−0.2 to 0.1 V vs. Ag/AgCl) associated with H_{upd} (underpotentially deposited hydrogen) processes ($H^+ + e^- = H_{upd}$), double-layer charging (0.1 to 0.3 V vs. Ag/AgCl) and oxide formation/reduction (0.3 to 1.3 V vs. Ag/AgCl) on the Pt surface.[30,47] As compared to the Pt/C sample, the hydrogen adsorption/desorption patterns of $Pt/CeO_2/C$ sample appear distinct and sharp. Studies show that the electrochemical hydrogen adsorption/desorption behaviour is highly dependent on the surface microstructure and surface properties of Pt crystallites. From the CV profiles, it is apparent that unlike in Pt/C, the Pt crystallites in the $Pt/CeO_2/C$ sample expose selective facets for interaction with H and other anions. Further, the characteristic hydrogen adsorption/desorption peaks in the H_{upd} regions of $Pt/CeO_2/C$ sample are more symmetrical which indicates more reversible Volmer reactions.[30] These results indicate the interfacial promoting activity of CeO_2 for electrochemical reactivity of controllably grown Pt with hydrogen.

Electrochemical active surface area (EAS) of Pt in both Pt/C and $Pt/CeO_2/C$ samples was estimated using the expression:[30,32]

$$\mathrm{EAS}\left(\mathrm{m^2 g^{-1}}\right) = \frac{Q_{\mathrm{H}}}{0.21 \times M_{\mathrm{Pt}}},$$

where Q_H is the Coulombic charge for hydrogen adsorption/desorption in the H_{upd} region, which is determined using the expression, $Q_H = 0.5\times (Q_{total} - Q_{DL})$, where Q_{total} is the total charge transfer in the H_{upd} region and Q_{DL} is the charge from double-layer region. The value 0.21 (in mC cm^{-2}) is the electrical charge associated with monolayer adsorption of hydrogen on Pt (assuming surface density of 1.3 × 1015 atoms cm^{-2}) and M_{Pt} is the Pt loading on the working electrodes (0.028 mg cm^{-2}). The EAS values of Pt in Pt/C and $Pt/CeO_2/C$ samples are found to be 42 and 48 m^2 g^{-1}, respectively. These results clearly show that irrespective

of similar Pt loading on each sample, the EAS of Pt for CeO_2-promoted Pt/C samples is higher than the bare Pt/C sample. This is ascribed to smaller size and high dispersion of Pt in the CeO_2-promoted Pt/C sample. Higher EAS suggests larger number of exposed active sites of Pt in CeO_2 promoted Pt/C sample.

3.3a *Catalytic activity study*: The ethanol electrooxidation reactions were performed on the Pt/C and $Pt/CeO_2/C$ sample electrodes in 0.5 mol L^{-1} H_2SO_4+ 1 mol L^{-1} C_2H_5OH solution, and the linear sweep voltammetry and chronopotentiometry results are presented in figure 11. As already known, the oxidation of ethanol to CO_2 involves multistep processes and many intermediates. A simple schematic of the electrooxidation of ethanol over a Pt catalyst can be presented as:[48]

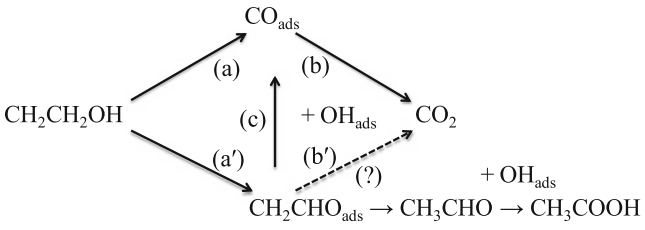

In linear sweep voltammograms, the broad peaks at positive current density correspond to electrooxidation of ethanol on the catalyst surface. Further, the

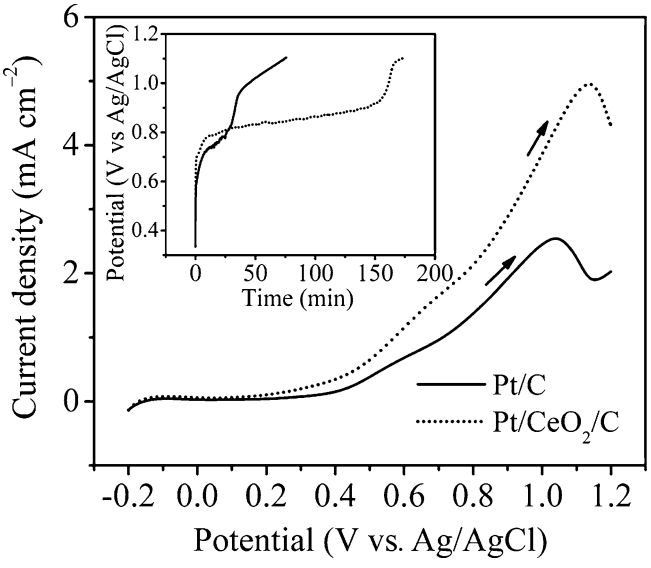

Figure 11. Cyclic voltammograms of Pt/C and $Pt/CeO_2/C$ sample electrodes in 0.5 mol L^{-1} H_2SO_4+ 1 M C_2H_5OH solution at a scan rate of 20 mV s^{-1}. Inset shows the potential vs. time (chronopotentiometry) profiles of Pt/C and $Pt/CeO_2/C$ sample electrodes in 0.5 mol L^{-1} H_2SO_4+ 1 M C_2H_5OH solution at a fixed current density of 15 mA cm^{-2}.

CeO_2-promoted Pt/C sample exhibits higher current density (4.9 mA cm^{-2}) than the bare Pt/C sample (2.5 mA cm^{-2}). During electrooxidation of ethanol, carbonaceous intermediates such as CO are prone to get adsorbed on the active Pt sites which hinder the activity of the catalyst. The adsorbed CO needs to be removed to regenerate the active site on Pt and this occurs by the following process:[30,35]

$$Pt - CO + H_2O \rightarrow CO_2 + 2H^+ + Pt.$$

Obviously, OH_{ads} species is necessary for the removal of adsorbed CO on Pt. In this context, CeO_2 provides ample OH_{ads} species through active triple-phase interfacial (interface between the Pt, oxide and the electrolyte) sites which promote oxidation of CO_{ads} on Pt/C via a synergic effect. This phenomenon is essential for improving the CO tolerance of the CeO_2-promoted Pt/C electrocatalysts. The mechanism of synergic effect is presented as follows:[30]

$$CeO_2 + H_2O \rightarrow CeO_2 - OH_{ads} + H^+ + e^-$$
$$Pt - CO_{ads} + CeO_2 - OH_{ads} \rightarrow Pt + CeO_2 + CO_2 + H^+ + e^-$$
and/or
$$Pt - CeO_2 + xCO \rightarrow Pt - CeO_{2-x} + xCO_2.$$

So, the linear sweep voltammetry results clearly demonstrate the promoting activity of CeO_2 to Pt/C for ethanol electrooxidation reaction.

The promoting and antipoisoning activity of CeO_2 to Pt/C for ethanol electrooxidation reaction was further confirmed from the chronopotentiometry measurements. Steady state measurements at a current density of 15 mA cm^{-2} were conducted on the $Pt/CeO_2/C$ and Pt/C samples, and the results are presented in the inset of figure 11. Typical chronopotentiometry profiles of both the samples show an increase in potential with time and finally jump to a limiting value due to oxygen evolution. The potential jump indicates poisoning of the catalyst surface and the longer time required for the potential jump is a measure of the better antipoisoning activity of the catalyst.[30,36] Chronopotentiometry profiles clearly show that the $Pt/CeO_2/C$ takes longer time for potential jump which clearly indicates better antipoisoning activity of CeO_2 promoted Pt/C sample compared to the bare Pt/C sample. Chronopotentiometry results show remarkable improvement in the antipoisoning activity of Pt/C by CeO_2 for electrooxidation of ethanol.

Improved electrocatalytic CO_{ads} oxidation efficiency of CeO_2-promoted Pt/C was ascertained from CO-stripping voltammetry study and the results are presented in figure 12.[30] The $Pt/CeO_2/C$ sample shows higher current response and a negative shift in the CO_{ads} electrooxidation peak potential compared to

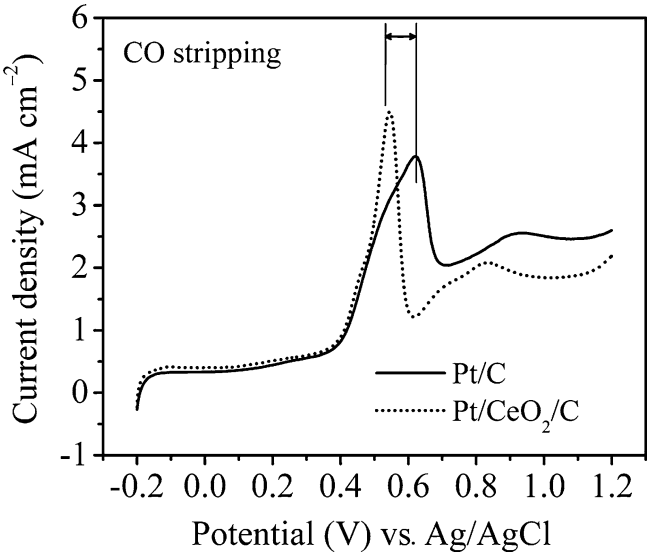

Figure 12. Comparative current response during electrochemical CO stripping (scan rate = 20 mV s^{-1}) on Pt/C and $Pt/CeO_2/C$ sample electrodes.

those observed for the Pt/C sample. These results indicate facile adsorption of OH_{ads} species on CeO_2 surface at lower potential which provide better electronic promoting activity to weaken the Pt-CO bond for CO electrooxidation. Further, the higher CO electrooxidation current density of $Pt/CeO_2/C$ sample leads to more number of OH_{ads} species on the CeO_2 surface which oxidize more CO_{ads} molecules to CO_2.[30] The CO-stripping voltammetry results are in absolute corroboration with the linear sweep voltammetry and chronopotentiometry results which altogether show significant promoting activity of CeO_2 to Pt/C for ethanol electrooxidation reaction in acidic media.

The findings reported here are crucial in the context of future development and exploitation of CeO_2 as well as other oxide-based catalysts with suitable microstructures for energy and environmental applications.

4. Conclusion

In conclusion, this study reports the versatility of homogeneous precipitation method to prepare CeO_2 with tuned surface morphologies and physicochemical properties. The first part of the study demonstrates the feasibility of reflux and hydrothermal mediated synthesis to prepare selective microstructures of CeO_2 with different reducibility and the morphology-controlled CO oxidation efficiencies of the prepared CeO_2 samples impregnated with 0.5 wt% Pt. The novel structured CeO_2 sample prepared by hydrothermal-mediated method shows low-temperature reducibility and superior CO oxidation efficiency compared to the bulk-like CeO_2 sample synthesized by conventional-reflux method. The next part of the study demonstrates that the surface morphology of CeO_2 can be easily tuned by different counter anions in the reaction medium under non-hydrothermal homogeneous precipitation conditions. Accordingly, nanorod and mesoflower morphologies of CeO_2 are synthesized taking nitrate and chloride as counter anions, respectively, in the reaction medium. Soot oxidation reaction on the as-prepared CeO_2 samples demonstrates morphology-dependent oxidation efficiencies of CeO_2; the CeO_2-nanorods being more efficient than the CeO_2-mesoflowers in oxidizing Columbian Carbon. This is attributed to Cl^- ion induced oxygen vacancies in CeO_2-nanorods which induce superoxide formation and oxygen spillover for facile oxidation of soot. In the last part of the study, the promotional effect of CeO_2 to Pt/C for ethanol electrooxidation reaction has been studied to address the significance of CeO_2 for energy-related application. The linear sweep voltammetry, chronopotentiometry and CO stripping voltammetry studies show that CeO_2 provides higher number of labile OH_{ads} species through active triple-phase interfacial sites for facile oxidation of CO_{ads} on Pt/C, and establish significant promoting and antipoisoning affect of CeO_2 to Pt/C for electrooxidation of ethanol in acidic media. By and large, the present study details the significance of surface properties of CeO_2 for energy and environmental applications.

Acknowledgements

We thank Ministry of New and Renewable Energy, New Delhi, for providing the CHI 7081C electrochemical workstation to carry out the electrochemical measurements and the SERC Division of DST, Ministry of Science and Technology, New Delhi, for providing powder XRD and BET facilities (under FIST Schemes). We also thank Prof. Paolo Fornasiero, Department of Chemistry, University of Trieste, Italy for CO oxidation measurements.

References

1. Setten B A A L, Makkee M and Moulijn J A 2001 *Catal. Rev. Sci. Eng.* **43** 489
2. Freund H, Meijer G, Scheffler M, Schlögl R and Wolf M 2011 *Angew. Chem. Int. Ed.* **50** 10064
3. Royer S and Duprez D 2011 *ChemCatChem* **3** 24
4. Herzing A A, Kiely C J, Carley A F, Landon P and Hutchings G J 2008 *Science* **321** 1331
5. Cargnello M, Wieder N L, Montini T, Gorte R J and Fornasiero P 2010 *J. Am. Chem. Soc.* **132** 1402

6. Bokhimi X, Zanella R and Angeles-Chavez C 2010 *J. Phys. Chem.* **C114** 14101
7. Bera P, Gayen A, Hegde M S, Lalla N P, Spadaro L, Frusteri F and Arena F 2003 *J. Phys. Chem.* **B107** 6122
8. Zhou H -P, Wu H -S, Shen J, Yin A -X, Sun L D and Yan C H 2010 *J. Am. Chem. Soc.* **132** 4998
9. Meher S K, Cargnello M, Troiani H, Montini T, Ranga Rao G and Fornasiero P 2013 *Appl. Catal.* **B130–131** 121
10. Ranga Rao G, Fornasiero P, Di Monte R, Kašpar J, Vlaic G, Balducci G, Meriani S, Gubitosa G, Cremona A and Graziani M 1996 *J. Catal.* **162** 1
11. Esch F, Fabris S, Zhou L, Montini T, Africh C, Fornasiero P, Comelli G and Rosei R 2005 *Science* **309** 752
12. Meher S K and Ranga Rao G 2012 *J. Colloid Interface Sci.* **373** 46
13. Si R and Flytzani-Stephanopoulos M 2008 *Angew. Chem. Int. Ed.* **47** 2884
14. Parida K M and Sahu N 2008 *J. Mol. Catal. A* **287** 151
15. Parida K M, Mohapatra P, Moma J, Jordaan W A and Scurrell M S 2008 *J. Mol. Catal.* **A288** 125
16. Parida K M, Sahu N, Tripathi A K and Kamble V S 2010 *Environ. Sci. Technol.* **44** 4155
17. Zhou K, Wang X, Sun X, Peng Q and Li Y 2005 *J. Catal.* **229** 206
18. Setiabudi A, Chen J, Mul G, Makkee M and Moulijn J A 2004 *Appl. Catal.* **B51** 9
19. Krishna K, Bueno-López A, Makkee M and Moulijn J A 2007 *Appl. Catal.* **B75** 189
20. Guzman J, Carrettin S and Corma A 2005 *J. Am. Chem. Soc*. **127** 3286
21. Carrette L, Friedrich K A and Stimming U 2001 *Fuel Cells* **1** 5
22. Lamy C, Lima A, LeRhun V, Delime F, Coutanceau C and Léger J -M 2002 *J. Power Sources* **105** 283
23. Song S, Maragou V and Tsiakaras P 2007 *J. Fuel Cell Sci. Technol.* **4** 203
24. Cameron D S, Hards G A, Harrison B and Potter R J 1987 *Platinum Met. Rev.* **31** 173
25. Lamy C, Belgsir E M and Léger J 2001 *J. Appl. Electrochem.* **31** 799
26. Cuesta A. 2011 *ChemPhysChem* **12** 2375
27. Yuan H, Guo D, Qiu X, Zhu W and Chen L J 2009 *J. Power Sources* **188** 8
28. Ranga Rao G, Justin P and Meher S K 2011 *Catal. Surv. Asia* **15** 221
29. Antolini E and Gonzalez E R 2010 *Appl. Catal.* **B96** 245
30. Meher S K and Ranga Rao G 2012 *ACS Catal.* **2** 2795
31. Suffredini H B, Tricoli V, Vatistas N and Avaca L A 2006 *J. Power Sources* **158** 124
32. Justin P and Ranga Rao G 2009 *Catal. Today* **141** 138
33. Justin P, Charan P H K and Ranga Rao G 2010 *Appl. Catal.* **B100** 510
34. Justin P and Ranga Rao G 2011 *Int. J. Hydrogen Energy* **36** 5875
35. Meher S K and Ranga Rao G 2013 *J. Phys. Chem.* **C117** 4888
36. Xu C and Shen P K 2004 *Chem. Commun.* 2238
37. Chu Y -Y, Wang Z -B, Jiang Z -Z, Gu D -M and Yin G -P 2011 *Adv. Mater.* **23** 3100
38. Bambagioni V, Bianchini C, Chen Y, Filippi J, Fornasiero P, Innocenti M, Lavacchi A, Marchionni A, Oberhauser W and Vizza F 2012 *ChemSusChem* **5** 1266
39. Meher S K, Justin P and Ranga Rao G 2011 *Nanoscale* **3** 683
40. Ranga Rao G 1999 *Bull. Mater. Sci.* **22** 89
41. Allian A D, Takanabe K, Fujdala K L, Hao X, Truex T J, Cai J, Buda C, Neurock M and Iglesia E 2011 *J. Am. Chem. Soc.* **133** 4498
42. Wang Z, Wang Q, Liao Y, Shen G, Gong X, Han N, Liu H and Chen Y 2011 *Chem. Phys. Chem.* **12** 2763
43. Issa M, Petit C, Mahzoul H, Aboukaïs A and Brilhac J -F 2009 *Top. Catal.* **52** 2063
44. Liu J, Zhao Z, Liang P, Xu C, Duan A, Jiang G, Lin W and Wachs I E 2008 *Catal. Lett.* **120** 148
45. Machida M, Murata Y, Kishikawa K, Zhang D and Ikeue K 2008 *Chem. Mater.* **20** 4489
46. Anumol E A, Kundu P, Deshpande P A, Madras G and Ravishankar N 2011 *ACS Nano* **5** 8049
47. Hu C -C and Liu K -Y 1999 *Electrochim. Acta* **44** 2727
48. Léger J -M, Rousseau S, Coutanceau C, Hahn F and Lamy C 2005 *Electrochim. Acta* **50** 5118